Delft University of Technology
Faculty of Applied Sciences

Bachelor of Science Thesis

Flow separation in non-Newtonian fluid flow through a diverging funnel

Author:
Paul Nollen

Supervisor:
Dr. Martin Rohde
Dr. Ntuthuko Hlongwa

August 19, 2019

Abstract

In this thesis, the flow of aqueous non-Newtonian fluids through a diverging funnel is examined for the purpose of designing a micro-scale test model for a semi-solid flow battery (SSFB). The aqueous electrolytes of SSFB's are non-Newtonian fluids meaning that they display non-regular viscoelastic properties. In particular, the electrolytes are pseudosplastics, meaning that they display shear-thinning behaviour. For research purposes, the desired design of the micro-scale test model for a SSFB should maintain a laminar flow without flow separation. This is because such a flow is predictable and easy to model. Therefore, the critical Reynolds number and critical volumetric flow rate, the point at which vortices start to develop, were sought for different divergence angles, and different shapes of the funnel. This was modeled for both the shear-thinning electrolyte and a standard Newtonian fluid in order to study the effect of shear-thinning fluid behaviour on flow separation. By modelling the micro-scale test model of a SSFB in COMSOL Multiphysics® the values for these sought parameters were determined.

A 'coarse' setting was chosen for the mesh considering both resolution and computation time. Values for the critical Reynolds number for both Newtonian and shear-thinning fluids were found and compared. The critical Reynolds number was found to be lower for pseudoplastics compared to Newtonian fluids which can be explained by the adverse pressure gradient. The results for different shapes of the funnel and cell did not show coherent results.

Through the obtained data a prototype for the micro-scale test model SSFB could be designed. The divergence angle of the funnel was chosen to be 25 degrees. This angle allows a wide range of volumetric flow rates for laminar flow and a relatively small volume of the funnel, meaning that less of the electrolyte is needed in the system. The design was slightly altered by shifting the inlets and outlets allowing the tubing to be properly connected to the cell.

For further research, it is recommended a finer mesh is applied for higher accuracy of the results. Futhermore, shear-thickening fluids and a combination of cell shapes and divergence angles are of of interest to study.

Contents

Chapter 1

Introduction

1.1 Renewable energy

1.1.1 General energy problem

Energy consumption is at an all time high. Humanity consumes over one million terajoules of energy per day, which is the equivalent of 3000 times the maximum daily output of the largest nuclear reactor in the world while running continuously [1]. Furthermore, estimations indicate that by 2040 energy consumption will have increased by circa 50%. With our fossil fuels running out, it is extremely important to change to other sources of energy production. Renewable energy sources such as wind, solar and hydro energy could be the answer, and therefore it is crucial to start exploring the possibilities of these solutions.

1.1.2 Energy storage problem

The growth of the worldwide demand for energy causes another concern, the need for cheap, safe and sustainable energy storage. Unfortunately, the peaks in productivity of renewables do not match the peaks in energy demand. Wind energy for example has maximum generation during the night in contrast to energy demand, which is significantly lower during the night. Solar energy generation has a maximum during the early afternoon, which does not match the usual peak in demand at the end of the afternoon. Sustainable energy storage could play a vital role in decoupling customer demand from energy generation [2]. The problem renewable energy faces is that (residential) energy storage systems are expensive and small-scaled at the moment. Currently, residences which make use of renewable energy generation systems only supplement the power that is provided by the grid. [3].

1.2 Stationary energy storage systems

Stationary energy storage systems (ESS) will play a pivotal role in the integration of renewable energy. Introducing ESS will not only be beneficial in order to create off-grid

energy systems, it has also been shown that incorporating widespread ESS in the usual power grid could yield a 4% reduction in energy use by 2030 [2]. In order to create a self-sustaining energy system, the storage has to meet a few demands. The storage needs to have a large capacity to store energy and the ability to deliver significant power when needed. Moreover, the storage should be cheap, reliable and most importantly safe [3].

1.2.1 Redox flow batteries

The redox flow battery (RFB) is a specific type of battery which relies on the principle of redox reactions. The design of an RFB has a major advantage compared to regular batteries. The system exists of external reservoirs containing the active materials, from where the fluid is pumped to an ion-exchange/electron-extraction power pack [4]. This means that the amount of energy stored in the system is decoupled from the power it delivers and thus can be scaled independently of one another. Furthermore, the RFB is able to charge/discharge more completely compared to other battery systems. On top of that is the RFB more safe compared to other storage systems since it does not emit harmful waste and is able to run at moderate to low temperatures. The lifetime is also relatively long for RFB's.

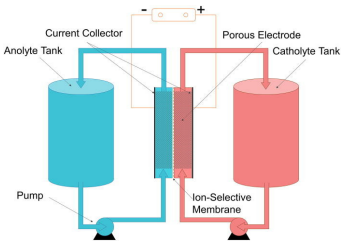

Figure 1.1: Schematic representation of a redox flow battery. [5]

1.2.2 Semi-solid flow battery

A limiting factor of the regular RFB is its energy density, which is relatively low. It is limited by electrolysis (which occurs above $1.5V$ cell voltage) and low ionic concentrations. Chiang et al. discovered in 2011 that by using suspension based electrodes the charge storage density of the flow battery solutions could be scaled up by ten times. This resulted in the design of the semi-solid flow battery (SSFB), which combines the advantage of designing flexibility and the high energy density of the active materials. It is desired that the electrolyte is properly mixed in order to create a homogeneous solution. This can be done by creating turbulence in the fluid flow, which happens at relatively high Reynolds numbers. However, due to the increased viscosity caused by the solid particles in the electrolyte the required pumping power has to be increased in order to create a fluid flow with similar magnitudes of the Reynolds number.

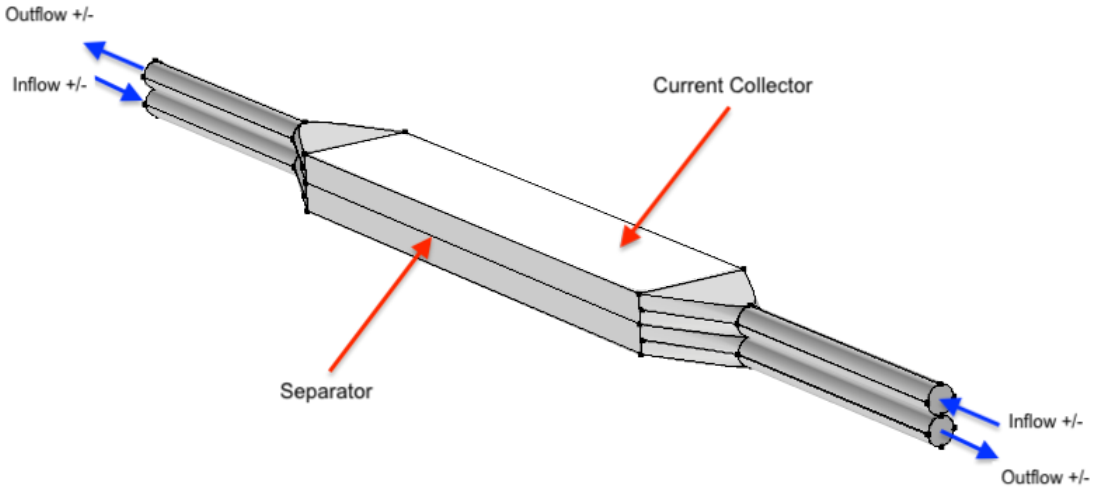

Figure 1.2: Schematic representation of a flow cell with diverging and converging funnels to the tubing.

1.3 Problem description

SSFB suspension electrodes are the subject of the research of the SEE and RPNM sections of the Reactor Institute Delft (RID). The sections are researching the optimal combination of suspension electrode mixtures for an SSFB, which will be tested in an experimental setup in which the efficiency of the electrolytes can be measured. The setup will resemble to a smaller scaled SSFB, however, there are differences. In order to measure the efficiency of the electrolytes, the flow needs to stay laminar because laminar flow is easy to model. This is in contrast to a normal scaled SSFB, where the flow is turbulent to accomplish proper mixing. The setup requires a diverging funnel from the tubing to the power cell, which is displayed in figure 1.2. The funnel is a critical section of the experimental setup, where a risk of flow separation development (vortices or steamlines) exists. Flow separation is undesirable because with vortices some of the fluid will not be able to flow properly through the cell, and such a flow is more complex to model. The fluids used in SSFB's are of a special type, namely non-Newtonian fluids. Non-Newtonian fluids display non-regular viscoelastic properties [6]. In order to determine an optimal divergence angle for experimental setup, the first question of interest is what effect the divergence angle of the funnel has on the flow of the electrolyte. Second of all, what is the effect of the shape of the cross section of the diverging funnel on the fluid flow of the non-Newtonian fluid.

1.4 Research goal

The overall objective of this research is to design an optimal experimental setup for the purpose of testing the efficiency of the electrochemical reaction with flowing electrolytes. In order to accomplish this goal, the following goals are pursued.

1. To examine the effect of the divergence angle of the funnel on the flow of the non-Newtonian fluid. At what *critical* Reynolds numbers and *critical* volumetric flow rates does flow separation occur for different divergence angles of the funnel. What is the effect of non-Newtonian behaviour compared to standard Newtonian behaviour of the fluid on the development of flow separation. Furthermore, at what point in the funnel does flow separation first occur.

2. To examine the effect of the shape of the cross section diverging funnel of the flow cell on the flow of the non-Newtonian fluid. At what *critical* Reynolds number does flow separation occur in the funnel for different shapes of the exit of the funnel with a constant hydraulic diameter, for both the electrolyte and a standard Newtonian fluid.

Both of the above goals will be pursued by modelling the flow cell with computational fluid dynamics (CFD) using COMSOL Multiphysics®.

1.5 Structure of thesis

The structure of the thesis consists of 7 chapters, starting with background information and a general overview of the research in chapter 1. Subsequently, the relevant theoretical framework will be layed out in chapter 2. In chapter 3 the experimental method will be shown, followed by the results and discussion of the results in chapter 4. Chapter 5 will display the design of the flow cell of the micro-scale test model for a SSFB. Lastly, conclusions will be drawn and recommendations will be made in chapter 6. The appendix provides additional information in chapter 7.

Chapter 2

Theoretical Background

In this chapter, the relevant theory for this research will be discussed. First the working principle of the SSFB will be explained, after which the electrolytes will be discussed. The rheology and flow of the electrolytes will be examined. Subsequently, the geometry of a diverging channel and its impact on the rheology will be discussed. Lastly, the theory behind computational fluid dynamics is explained.

2.1 Working principle SSFB

As for all RFB's, the principle on which the energy storage of an SSFB relies is that of redox reactions.

2.1.1 Redox reaction

The word redox is a combination of the words *reduction* and *oxidation*. A redox reaction is a reaction between two different molecules, where an exchange of electrons takes place. There is always one molecule, the *reductor*, that donates one or multiple electrons to the other molecule, the *oxidator*. The chemical reactions are drawn up by combining the two half reactions. The process of a redox reaction is depicted schematically in figure 2.1.

1. $Reductor \longrightarrow Reactant\ 1 + e^-$ (oxidation)
2. $Oxidator + e^- \longrightarrow Reactant\ 2$ (reduction)

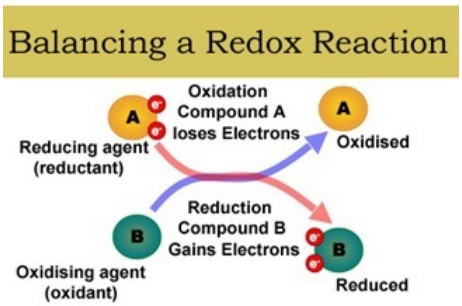

Figure 2.1: Schematic representation of the concept of a redox reaction [7]

An electrolyte through which the electrons and ions can freely move is necessary for the reaction to take place. The reaction can be reversed by applying a voltage, which makes an ideal basis for a battery to store energy.

2.1.2 Energy conservation

In an SSFB, the electrodes are aqueous, which means that the reducting agent and the oxidizing agent are dispersed in an electrolyte. These are the anolyte (negative electrolyte) and the catholyte (positive electrolyte). The principle is as follows. The fluids flow alongside each other in a cell (the flowcell), where they are separated only by a separator. The separator is a membrane which only allows ions to be exchanged across it. During discharge, the ions cross the membrane from the anolyte to the catholyte. This causes a current of electrons, or in other words, electricity.

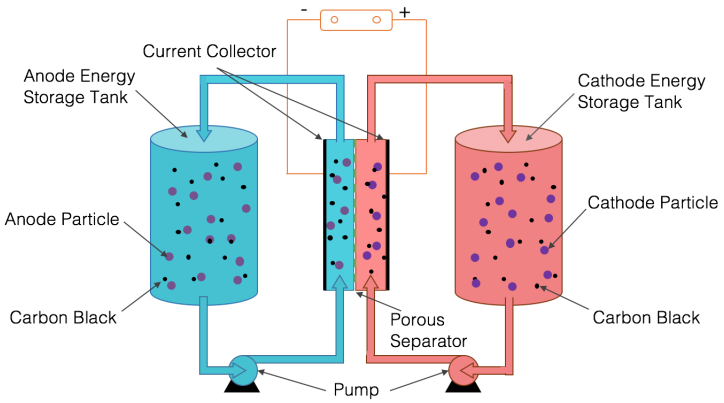

Figure 2.2: Schematic representation of a semi-solid flow battery. [5]

The battery charges by applying a voltage, which causes the ions to diffuse back over the membrane to the anolyte. Besides the flow cell, the SSFB systems consists of external tanks, both for the anolyte and catholyte. This way, the total amount of energy in the system can be scaled independently of the power it delivers through the

flow cell. Ideally, there is no energy loss between charging and discharging [3]. However, the suspensions have to be pumped through the systems, which costs more pumping power due to the higher viscosity compared to solutions [2].

2.2 Slurry electrodes

The difference between the regular RFB and the SSFB is that the flowable electrolytes in SSFB's are suspensions instead of solutions. The major advantage with suspension electrodes, or slurry electrodes, compared to solutions is that the energy volume density is up to 10 times higher due to the much greater energy density inherent to solid-storage compounds. [4].

The slurry electrodes consist of 3 components, namely the active material, carbon black and the electrolyte in which the other two components are dispersed. In weight percentages, the slurry electrodes will consist of 60% electrolyte, 30% active material and 10% carbon black [8]. The slurry electrodes are *pseudoplastics* which is a form of non-Newtonian fluids. Non-Newtonian fluids and their behaviour will be discussed in the section 2.3.

2.2.1 Electrolyte

The electrolyte is a fluid in which the solid particles of the active material and the carbon black are dispersed. The electrolyte is used to transport the charge carriers, the ions, and to transport the active materials through the system by convection. The electrolyte used both for the anolyte and catholyte is $LiNO_3$ [8].

2.2.2 Redox active compounds

In the present of writing this thesis, the definite combination of active materials for the anolyte and catholyte is not yet determined. The active material for the catholyte is already determined to be $LiMn_2O_4$ (LMO). The active material for the anolyte is not yet determined. However, Li_2TiO_3 currently shows the most promising results as the active material for the anolyte [8].

2.2.3 Conducting percolated network of carbon particles

Carbon black is the third component of the slurry electrodes. The function of carbon black is to increase the conductivity of electrons in the electrolyte. It works by forming a percolating network of carbon particles, which enhances both electronic and ionic conduction [9][10]. The percolation theory suggests that above a certain threshold a conductive network can be formed. The conducting network of carbon particles replaces the porous carbon electrode used in older designs of RFB's, reducing the needed pump power to maintain a continuous flowing system.

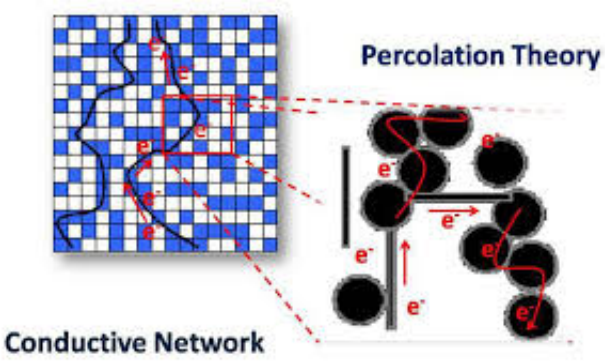

Figure 2.3: Schematic depiction of the percolation network of carbon particles [11].

2.3 Rheology

As mentioned in the previous section, the suspension electrodes display non-Newtonian behaviour, namely shear-thinning or *pseudoplastic* behaviour. Non-Newtonian refers to the unusual viscoelastic properties they have compared to 'normal' Newtonian fluids. These differing properties have an influence on the flow and velocity profile. Non-Newtonian liquids can be categorized in different categories according to their relation between the shear stress and velocity gradient. The study of these kind of properties is called *rheology* [12]. For the purpose of testing the electrochemical reaction with flowing electrolytes the rheology is important. The flow needs to stay laminar without vortices for the experimental setup. The rheology is not as significant for eventual upscale models of the SSFB because there the flow will be turbulent.

2.3.1 Non-Newtonian fluids

The three main categories for non-Newtonian fluids are the fluids which display shear-thinning viscosity (pseudoplastics), fluids which display shear-thickening viscosity (dilatant) and fluids which only start to flow once a minimum amount of shear stress is exerted on them (Bingham liquids). Examples are: ketchup (shear-thinning), cream (shear-thickening) and toothpaste (Bingham liquid) [12]. The different relations between shear stress and the shear rate are displayed in figure 2.4.

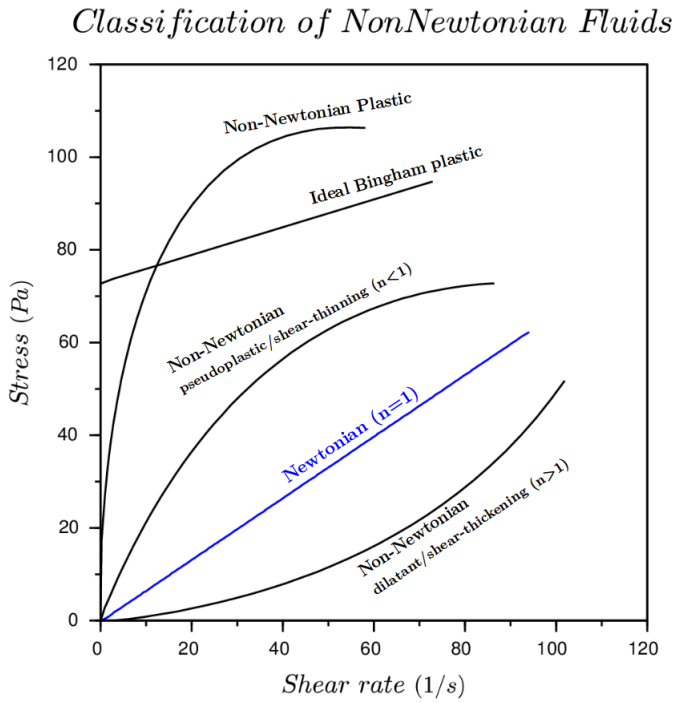

Figure 2.4: The relation between shear stress and velocity gradient for different fluids [13].

Pseudoplastics, dilatant and, as a special case, Newtonian fluids obey the $Ostwald-De\,Waele$ or the *power law* model, which links the shear stress and velocity gradient of the fluid.

$$\tau_{ry} = -K \mid \frac{dv_y}{dr} \mid^{n-1} \frac{dv_y}{dr} \tag{2.1}$$

In the above equation τ_{ry} $[\frac{N}{m^2}]$ is the shear stress. $\frac{dv_y}{dr}$ $[\frac{1}{s}]$ represents the velocity gradient and if the modulus is taken, the *shear rate*. K $[Pa\,s]$, which is a constant, represents the *consistency* and n $[-]$ the $flow\,index$, which is also a constant. The flow index determines in which category the fluid can be placed. For $n < 1$, the fluid displays shear-thinning behaviour. For $n > 1$ the fluid displays shear-thickening behaviour. Notice that if $n = 1$ the fluid is a Newtonian fluid. In the case that a fluid is described by an $n \neq 1$, the *apparent* viscosity is not a constant, in contrast to Newtonian fluids. This can be observed in the figure above, where the slope of the line represents the (apparent) viscosity of the different kind of fluids [14].

$$\mu_{app} = K * \dot{\gamma}^{n-1} \tag{2.2}$$

Where $\dot{\gamma} = \mid \frac{dv_y}{dr} \mid [\frac{1}{s}]$ is referred to as the shear rate. μ_{app} $[Pa\ s]$ is the apparent viscosity.

2.3.2 Shear-thinning fluid flow

Consider a fluid which flows through a circular pipe. After a certain length, the *entrance length*, the velocity profile of a fluid is fully developed for laminar flow. This velocity profile is parabolic for Newtonian fluids, however, for non-Newtonian fluids the velocity profile has different shapes.

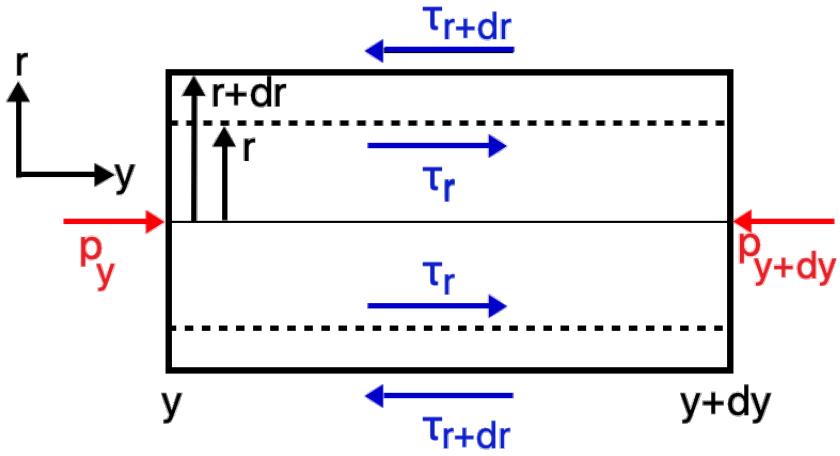

Figure 2.5: Schematic representation of the forces acting on a control volume of fluid in a pipe.

As is schematically displayed in figure 2.5, a control volume of fluid in a pipe has several forces acting on it. There is pressure on both cross-sections and it experiences shear stress on its sides. In order to derive an equation for the velocity profile, first the force balance has to be established.

$$0 = p\mid_y 2\pi r dr - p\mid_{y+dy} 2\pi r dr + 2\pi(r\tau_{ry})\mid_r dy - 2\pi(r\tau_{ry})\mid_{r+dr} dy \tag{2.3}$$

In this equation p $[Pa]$ represents the pressure. After simplifying and rearranging this equation, it can be set equal to equation 2.1. The following equation is derived:

$$\frac{dv_y}{dr} = (\frac{1}{2 * K}\frac{dp}{dy})^{\frac{1}{n}} r^{\frac{1}{n}} dr \tag{2.4}$$

Equation 2.4 can be integrated over r, after which the boundary condition that at the walls the velocity is equal to zero is applied. After simplification again, the following equation describes the velocity profile of a non-Newtonian fluid through a pipe [14].

$$v_y(r) = (\frac{1}{2 * K}\frac{dp}{dy})^{\frac{1}{n}}(\frac{n}{n+1})R^{1+\frac{1}{n}}[1 - (\frac{r}{R})^{1+\frac{1}{n}}] \tag{2.5}$$

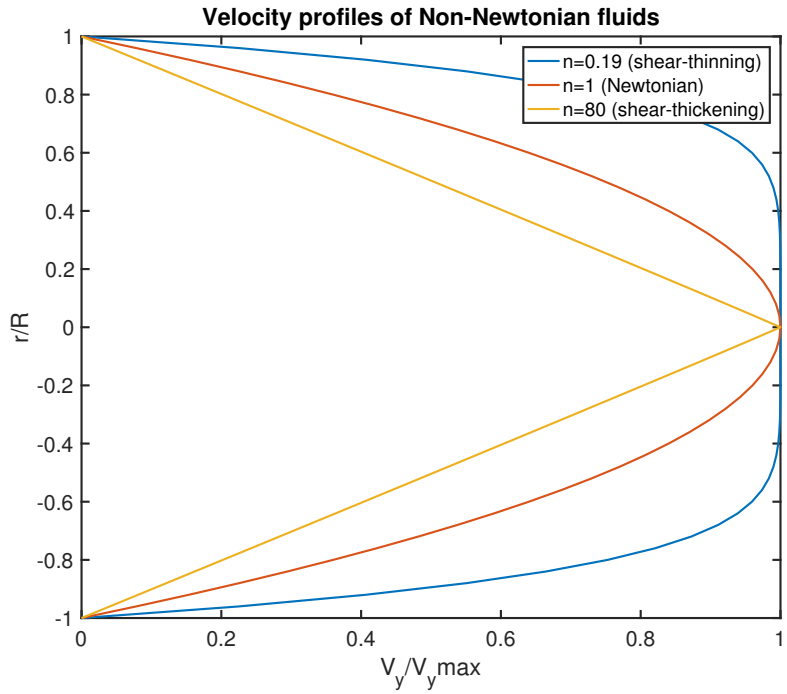

Figure 2.6: Plot of the laminar velocity profiles of 3 different types of fluids between two plates.

The velocity profile is parabolic for Newtonian fluids ($n = 1$) with the maximum velocity on the axis of the cylinder ($r = 0$). The average velocity for Newtonian fluids is exactly half of the maximum velocity. However, notice how a change in the flow index number n results in a significant change of the velocity profile. This is illustrated in figure 2.6. As the flow index number n starts to decrease, the velocity profile becomes less sharp and more blunt and starts to approach the profile of ideal plug flow [12]. On the contrary, as the flow index number starts to increase, the velocity profile becomes 'sharper'.

2.3.3 Geometry influence on rheology

For a pseudoplastic fluid such as the electrolytes used for SSFB's, the flow index number n is smaller than 1. This means that in equation 2.2 the exponent of the shear rate $\dot{\gamma}$ is a negative number. By rewriting equation 2.2 with $m = 1 + n$ the following equation can be derived, where m is always a positive number for pseudoplastics.

$$\mu_{app} = \frac{K}{\dot{\gamma}^m} \tag{2.6}$$

This equation shows that when the magnitude of the velocity gradient, the shear rate, is high, the viscosity will be low and thus the fluid will flow more easily. For a pipe, the apparent viscosity will be lowest near the sides of the pipe, where the magnitude of the velocity gradient is the greatest. The viscosity profile over a surface of the pipe will look similar to the velocity profile for $n < 1$ as shown in figure 2.6. However, for shapes such as rectangles, the apparent viscosity can differ significantly over the surface. This is of importance for the shape of the cross section of the funnel.

2.4 Fluid flow through a diverging channel

As mentioned in the introduction, the flow in the experimental setup for the micro-scale test model of a SSFB has to stay laminar and without vortices in order to properly study the diffusion and reactions of the active materials within the electrolytes. In fluid flow, the ratio between the convective transport and the molecular transport is an important dimensionless quantity used to help predict flow patterns in fluid flow situations. This ratio is a dimensionless number called the *Reynolds* number.

$$Re = \frac{\rho < u > D_h}{\mu} \tag{2.7}$$

Where ρ $[\frac{kg}{m^3}]$ represents the density of the fluid, u $[\frac{m}{s}]$ represents the average flow velocity magnitude and μ $[Pa\,s]$ represents the (apparent) viscosity. D_h $[m]$ represents the hydraulic diameter of the channel in which the fluid flows. D_h is defined as 4 times the surface A $[m^2]$ of the channel divided by the perimeter S $[m]$ of the channel.

$$D_h = \frac{4A}{S} \tag{2.8}$$

Typically, for pipe flow, the flow enters the transition from laminar to turbulent flow at $2000 < Re < 2500$ [12]. The *critical* Reynolds number is the number where transition from laminar to turbulent flow starts, so in the case of water flowing through a pipe the critical Reynolds number is 2000.

For pseudoplastics, such as the electrolytes used in the SSFB, the Reynolds number is a complicated number since the viscosity depends on the geometry of the channel and the local flow velocity gradients.

2.4.1 Flow separation

Instabilities in laminar flow occur for much lower Reynolds numbers when convergences and divergences are implemented in the channel. As was already shown in 1966, a wall-divergence of less than a degree brings down the Reynolds number where flow

separation starts to occur by an order of magnitude [15]. Conversely, a convergence strongly stabilizes the flow [16].

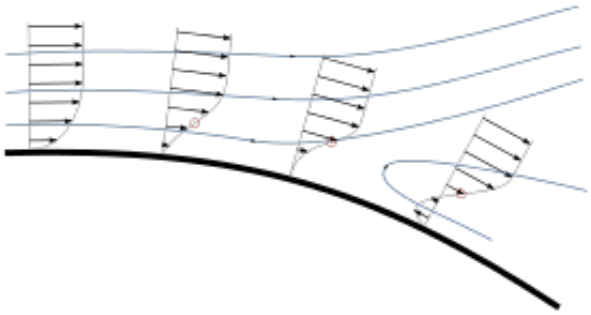

Figure 2.7: Schematic representation of flow separation in a diverging channel []

In a diverging channel, when a certain value for the Reynolds number is reached, laminar vortices appear. This form of *flow separation* is called *boundary layer separation*, which is schematically displayed in figure 2.7. Flow separation occurs when the boundary layer travels far enough against an *adverse pressure gradient*. An adverse pressure gradient means that the pressure has a positive gradient $\frac{dp}{dy}$ over some length of flow. The pressure at the walls at the beginning of the funnel has this adverse pressure gradient. When large enough, this adverse pressure gradient causes the flow velocity close to the walls to drop to (almost) zero. Subsequently, the flow detaches from the walls, and vortices or streamlines of slow negative flow velocity are formed [17]. These vortices are undesirable for the SSFB since some of the electrolytes will not be flowing through the flowcell. Furthermore, vortices are a complicating factor in the flow and thus more complex to model. The Reynolds number from which vortices start to form in a diverging channel is subject of this study.

2.4.2 Divergence angle influence on critical Reynolds number

As mentioned in the previous subsection, the critical Reynolds number drops by an order of magnitude for a divergence of less than one degree. However, there is not yet a clear understanding what the critical Reynolds number is for different angles of divergence. The critical Reynolds number for diverging channels was the subject of several studies, however, most of them only consider small angles of divergence [17]. In 2015, Jotkar et. al studied the critical Reynolds number for 2D divergent channels at greater angles. In figure 2.8 the results of Jotkar et. al and results of earlier studies are depicted. The ϵ [-] represents the incline in height of the divergence over a length of $L = 5$ [-].

$$\tan\alpha = (\frac{\epsilon}{L}) \tag{2.9}$$

For example, $\epsilon = 0.1$ means a divergence angle of a little over 1 degree, whereas $\epsilon = 1$ means a divergence angle α [degrees] of a little over 11 degrees. The graph clearly

shows that as the divergence angle increases, the critical Reynolds number decreases very strongly. However, it is still not exactly predictable at what Reynolds number flow separation starts to occur for all angles. The study of Jotkar et. al showed that for a divergence where $\epsilon = 2.3$, meaning an angle α of 24.7 degrees, vortices start to appear for a value of around 8 for the Reynolds number [16]. Notice however that this is modeled with a constant viscosity and in 2D.

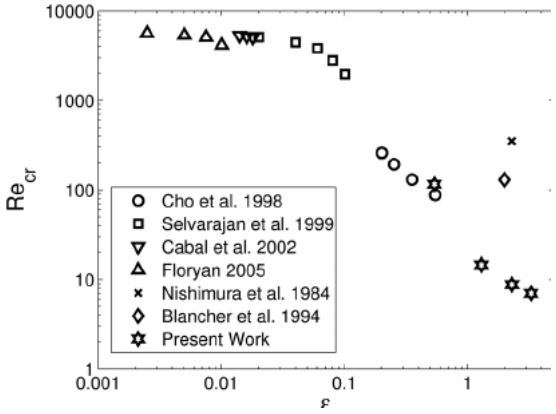

Figure 2.8: Critical Reynolds numbers for differing angles found by several studies. The x-axis shows the value of vertical rise ϵ over a length $L = 5$ from which the angle can be calculated [16].

2.5 Computational fluid dynamics

Computational fluid dynamics (CFD) is a field of fluid mechanics that uses numerical analysis to solve fluid flow problems. CFD relies on *discretization methods*. Examples of discretization methods are the $finite\ volume$, $finite\ element$ and $finite\ difference$ method. The program used to model the subject of the research, COMSOL Multiphysics®, uses the finite element method (FEM).

FEM is usually applied to heat transfer, fluid flow and mass transport problems. It solves these problems by dividing the domain into small parts which are called the finite elements. The larger the number of finite elements used to subdivide the domain, the higher the quality of the mesh, or resolution. FEM then solves a system of algebraic equations for every node to approximate unknown functions or variables over the total domain. Boundary conditions are applied in order to obtain a numerical answer for the problem [12].

In fluid flow problems, CFD will evaluate the (continuous) Navier-Stokes equations for every node in the mesh in order to predict the flow after which it approximates the unknown functions over the domain.

$$\rho\frac{\partial \mathbf{v}}{\partial t} + \rho(\mathbf{v}\cdot\nabla)\mathbf{v} = \mu\nabla^2\mathbf{v} - \nabla p + \rho\mathbf{g} \tag{2.10}$$

In the Navier-Stokes equations, ρ $[\frac{kg}{m^3}]$ is the density, $\mathbf{v}$ $[\frac{m}{s}]$ is the velocity vector, μ is the viscosity $[Pa\ s]$, p is the pressure $[Pa]$ and $\mathbf{g}$ $[\frac{m}{s^2}]$ is the gravity vector.

If a computer does not have a large amount of computing power or memory, the number of volume elements can be reduced by selecting a coarser grid. This means that there are less nodes where variables are evaluated, leading to a less accurate or even unphysical solution of the problem.

Chapter 3

Experimental method

In the following chapter, the experimental methods used to conduct this research will be explained. The focus lies on the flow of the electrolyte through the flow cell, including the diverging and converging funnel. First, the design of the model will be discussed, including geometry and boundary conditions. Second, the properties of the modelled fluid will be examined, after which the mesh will be discussed. Lastly, the simulation method will be explained.

3.1 Model development

In this section, the geometry of the model will be discussed. In order to determine whether, when and at what point flow separation occurs, a half flow cell is modeled in COMSOL Multiphysics®.

3.1.1 Dimensions flow cell

The shape of the half flow cell is that of a matchbox, a stretched out geometry with a constant rectangular surface. Compared to previous studies, the dimensions of the half flow cell in this research are slightly bigger [18] [19] [20]. The length of the cell is 10cm, the width 2cm and the height 0.5cm (volume of 10mL). These dimensions were chosen based on previously conducted studies [19], the constraint of a maximum amount of electrolytes (100mL per electrolyte) and in consultation with Wonderboy [8].

The system requires both a diverging and converging funnel in order to connect the flow cell to the tubing. The tubes modelled have an inner diameter of 0.5cm, the same height as the flow cell. The funnel has an odd shape, changing shape from a circular to a rectangular surface. The divergence angle is one of the subjects of this study. Therefore, the divergence angle, and thus the length, of the funnel will be varied in order to study at which volumetric flow rates flow separation will develop for each specific divergence angle. The converging funnel has the exact same dimensions as the diverging funnel, in

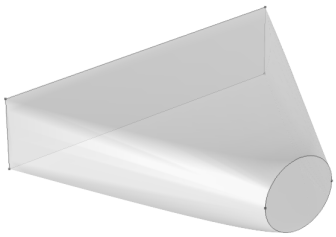

Figure 3.1: Schematic representation of the funnel.

order to both study parallel flow and non parallel flow. However, the converging funnel is not subject of the study, since convergences strongly stabilize the flow [16].

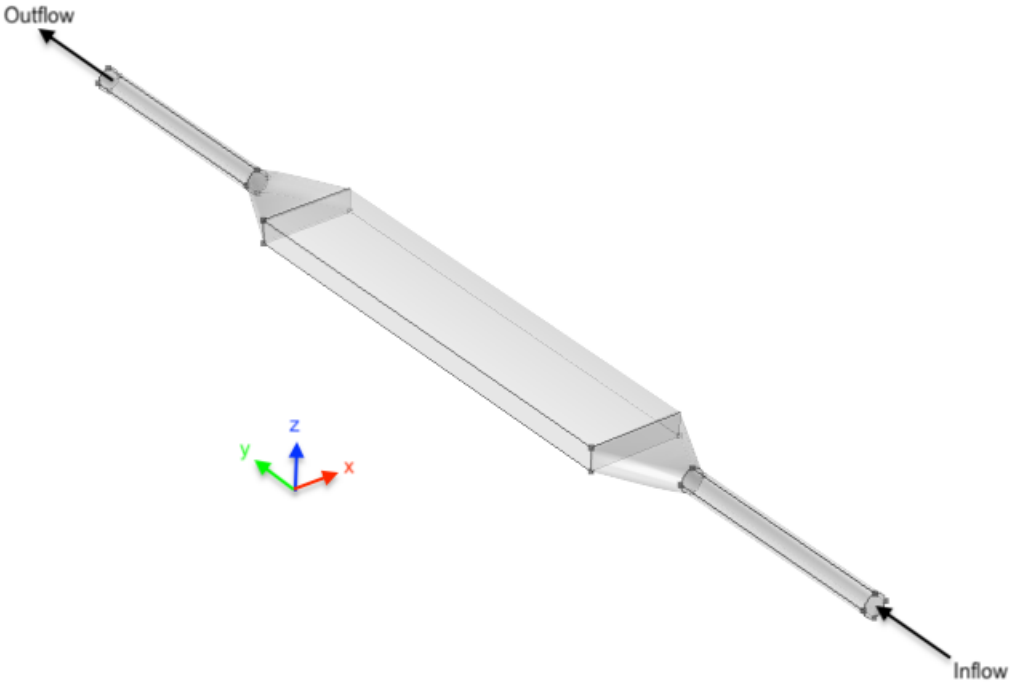

Figure 3.2: Schematic depiction of the half flow cell model.

Besides the half flow cell and the diverging and converging funnels, there is also a small part of the tubing modelled in order to simulate the real system as precisely as possible. The tubes have an inner diameter of 0.5cm, and both a length of 5cm. The complete geometry which will be modeled can be observed in figure 3.2. Notice the axis and direction of flow.

3.1.2 Boundary conditions

As inlet boundary, a laminar inflow is applied. The volumetric flow rate ϕ_v $[\frac{m^3}{s}]$ determines the amount of electrolyte which flows through the model. The laminar inflow is fully developed, ensuring a fully developed laminar velocity profile for the electrolyte. As an outlet boundary condition, the applied pressure at the outlet is $p = 0$ $[Pa]$.

Furthermore, a no-slip boundary condition is applied to all the walls of the model. This means that at all the walls, the relative velocity between the fluid and solid wall is zero. In this case, that means that the fluid velocity at the walls is equal to zero.

3.2 Fluid properties

As mentioned in the previous chapter, the electrolytes are non-Newtonian fluids, namely fluids that display shear-thinning or pseudoplastic behaviour. The viscosity of these fluids is not constant, and can be calculated with equation 2.3.3. The value for the flow index is $n = 0.192876$ [-], the value for the flow consistency is $C = 13.1238$ $[Pa\ s]$ and the density is $\rho = 1000$ $[\frac{kg}{m^3}]$. These values were selected from the papers where the SSFB was first modeled [4][6]. However, these values were used for a specific percentage combination of active material, electrolyte and carbon black. It is therefore possible that these values differ slightly for the specific electrolyte which will be used in the experimental setup.
Moreover, the fluid is assumed to be an incompressible fluid, meaning that the density of the fluid is constant within an infinitesimal volume that moves with the flow velocity.

3.3 Mesh

As mentioned in the previous chapter, COMSOL Multiphysics® uses the finite element method. The modeled geometry is divided in a finite number of elements, or cells. The nodes of the mesh are individually evaluated in order to determine local variables, which is important in order to define when flow separation starts to develop. The number, shape and location of cells is called the mesh that is applied.

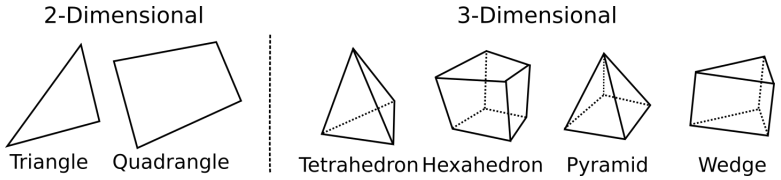

Figure 3.3: Schematic depiction of several mesh cell type shapes. [21]

The cells of the mesh are divided into several different shapes. The most used cell type is the tetrahedron, followed by prisms (wedges), triangles and in significantly lower amounts quads (hexahedrons). At the walls, the mesh has a finer grid and thus a higher resolution in order to study flow separation optimally.

3.4 Simulations

In this section, the research method will be discussed. The approach to determine flow separation will be explained, in combination with the variables that are varied.

3.4.1 Angle variation

In order to observe the effect of the divergence angle on the critical Reynolds number, the divergence angle will be varied from θ_d =1 to 45 degrees, in steps of 1 degree. Since the mesh depends on the geometry, for every single divergence angle a new mesh has to be applied in order to properly study the flow.

3.4.2 Determination flow separation

Flow separation occurs when vortices within the flow appear, thus flow with negative velocity streamlines in the flow direction. To determine where vortices start to develop, the minimum velocity of flow in the flow direction in the funnel is evaluated by using the *volume minimum* function of COMSOL Multiphysics®. This function evaluates the total volume of the funnel for the minimum local velocity. The volumetric flow rate ϕ_v $[\frac{m^3}{s}]$ is increased until a negative velocity in the y-direction (direction of flow, see figure 3.2) is found by the volume minumum function.
Subsequently the funnel is divided into zx-slices to determine at what length in the funnel the flow separation starts to appear, the separation point. The slice at which the flow separation arises is then used to determine the hydraulic diameter D_h $[m]$. Furthermore, the average velocity $< u >$ $[\frac{m}{s}]$ magnitude and the average apparent viscosity $< \mu >$ $[Pa\ s]$ is evaluated for the slice by integrating over and dividing by the surface of the slice. Combining these variables with the density ρ $[\frac{kg}{m^3}]$, the critical Reynolds number for when flow separation starts to develop can be calculated by using equation 3.1.

$$< Re >= \frac{\rho < u > D_h}{< \mu >} \tag{3.1}$$

The method is illustrated in figure 3.4, where the critical Reynolds number is determined for a divergence angle of 25 degrees.

3.4.3 Cell shape variation

Another subject of the study is to examine the influence of the shape of the flowed through surface on the critical Reynolds number. For that purpose, the shape of the flow cell is varied. As can be seen in figure 3.5, the hydraulic diameter of the flow cell can be calculated through the width and height of the cell. In order to study the influence of the shape, the hydraulic diameter and divergence angle is kept constant (respectively 0.8cm and 25 degrees), but the ratio of the height and width is varied. The variable $x = \frac{width}{height}$ is varied in steps of 0.5 from 1 (square surface) to 4. The upper limit is chosen as 4, because for higher values of x, the height of the cell would be smaller than the diameter of the tubing, which would mean a partly converging funnel. The critical

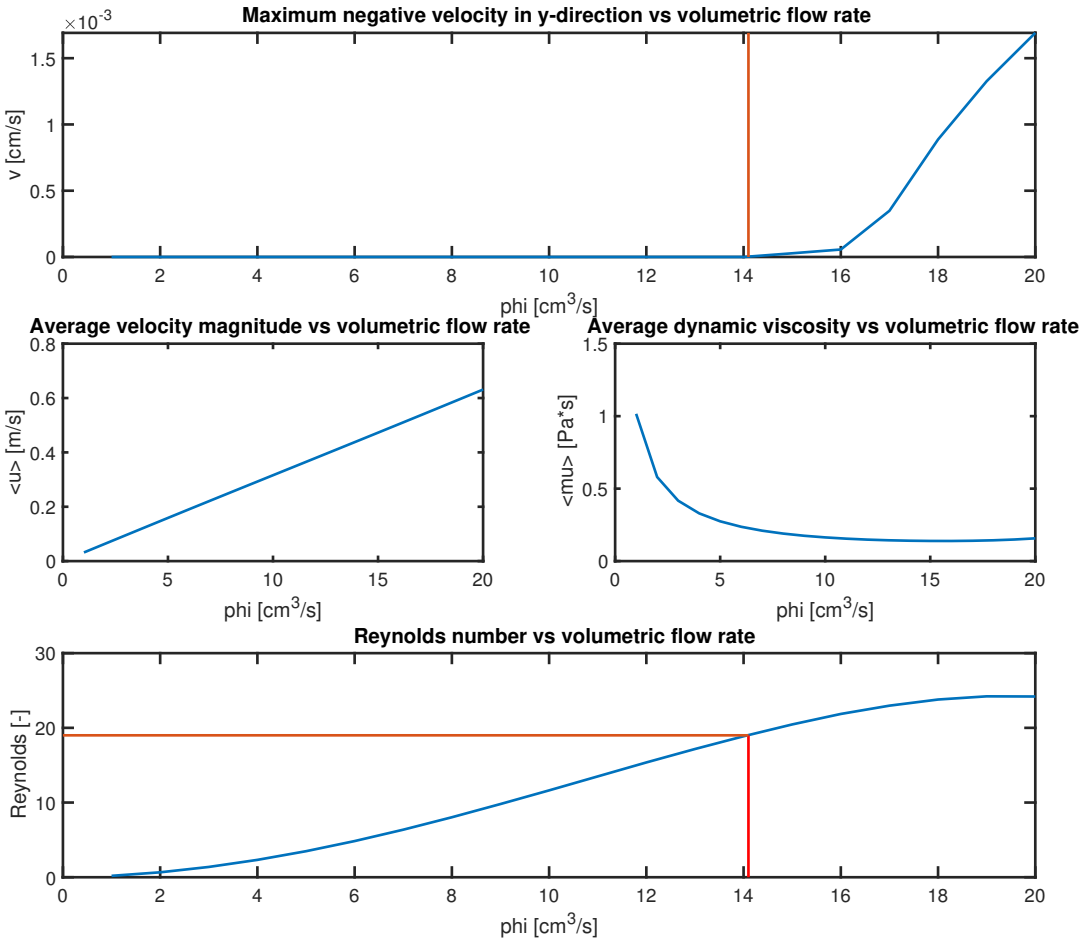

Figure 3.4: Plots of the variables used in the calculation for the Reynolds number. First plot it the negative y-velocity, second the average velocity magnitude, third average dynamic viscosity and last the Reynolds number, all against different volumetric flow rates.

Reynolds number is calculated by applying the same approach as in the previous section. Moreover, the critical Reynolds number is also examined for the hypothetical case of a cylinder flow cell with the same hydraulic diameter.

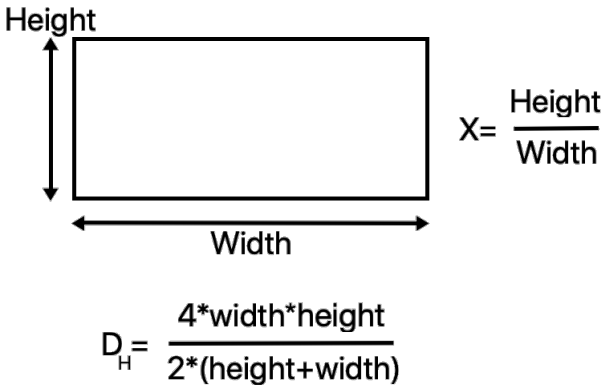

Figure 3.5: Schematic depiction of the flow cell surface plus the calculation of the hydraulic diameter and variable x.

Chapter 4

Results and discussion

In this chapter the results of the conducted research will be presented, together with a physical discussion about these results. The chapter starts with the selection of the mesh, followed by the results obtained by varying the divergence angle. Subsequently, the impact of hydraulic diameter variation will be examined.

4.1 Mesh selection

The mesh is a crucial part of CFD. Naturally, the highest resolution should be aspired in order to obtain a solution which has high accuracy. However, CFD is very demanding in terms of computation power and time, especially as the resolution of the grid increases. In this section, several qualities of resolution are evaluated in terms of accuracy and computation time for the purpose of selecting the best achievable mesh for modeling the flow cell.

4.1.1 Resolution comparison meshes for relatively low Reynolds numbers

COMSOL Multiphysics® has 9 different default settings for the resolution of the mesh. They range from extremely coarse to extremely fine. In order to select the best mesh for this research, the critical Reynolds number was evaluated for a geometry of a divergence angle of 10 and 25 degrees. These divergence angles were chosen for the purpose of studying the differences due to mesh resolution for both relatively high and low Reynolds numbers. The results for relatively low Reynolds numbers (divergence angle of 25 degrees) are illustrated in table 4.1.

As can be seen from the table, as the resolution increases from extremely coarse to fine, the critical Reynolds number converges to roughly 19. For an extremely coarse mesh, the solution for the critical Reynolds number deviates strongly. The solution found using a coarse mesh is fairly near to the solution using a fine mesh.

Table 4.1: Mesh resolution comparison for a divergence angle of 25 degrees

Mesh	ϕ_v $[\frac{cm^3}{s}]$	$<\mu>[Pa\ s]$	<u>$[\frac{m}{s}]$	Critical Reynolds[-]
Extremely coarse	18.5	0.13500	0.60235	26.86
Extra coarse	16.4	0.15105	0.52913	21.09
Coarser	17.6	0.15242	0.55472	21.91
Coarse	14.1	0.14075	0.4423	19.01
Normal	15.3	0.14544	0.48015	19.11
Fine	15.3	0.14943	0.48145	19.10

4.1.2 Resolution comparison meshes for relatively high Reynolds numbers

Table 4.2 illustrates the mesh resolution comparison for the solution of a divergence angle of 10 degrees. Unfortunately, the critical Reynolds number does not show a clear convergence to a certain value for a higher resolution of the mesh.

Table 4.2: Mesh resolution comparison for a divergence angle of 10 degrees

Mesh	ϕ_v $[\frac{cm^3}{s}]$	$<\mu>[Pa\ s]$	<u>$[\frac{m}{s}]$	Critical Reynolds[-]
Extremely coarse	62.4	0.072819	2.1397	176.89
Extra coarse	30.3	0.11399	0.9593	50.66
Coarser	40.3	0.11256	1.2814	68.53
Coarse	35.6	0.09931	1.1186	68.09
Normal	27.3	0.11067	0.85572	46.55
Fine	36.6	0.12082	1.1477	57.19

4.1.3 Computation time and selection

The research was conducted by applying simulations using a desktop computer at the RID and a personal laptop. The resolution of the mesh is extremely important in the conducted research, since the flow separation develops at very specific points in the funnel. However, in order to obtain solutions with the highest possible resolution, a mesh had to be selected considering not only resolution, but also computation time. The computation time needed to complete one single simulation increased enormously as the resolution of the mesh increased. Notice that the highest tested resolution is fine, which is because both computers were unable to complete one single simulation for a finer mesh in one weekend while running continuously (!). The fine mesh took at least 8 hours to complete one single simulation.
The selection of the mesh was based on both quality of the solution, computation time and the range of critical Reynolds numbers that were sought. Considering all of these factors, the 'coarser' mesh was selected as the resolution. Reasons for the selection were that the majority of the sought critical Reynolds numbers are expected to be relatively

low, the computation time for one single simulation is reasonable (circa 15 minutes) and the quality of the solution is acceptable.

4.2 Angle dependence flow separation

This section will discuss the influence of the divergence angle on the flow separation by presenting results of the conducted research. First the point of detachment of flow will be examined, after which the critical Reynolds number of the fluid for different divergence angles will be presented together with a comparison to Newtonian fluids.

4.2.1 Separation point

As mentioned in chapter 2, boundary layer separation is caused by an adverse pressure gradient which exerts pressure on a flow. The point the flow detaches from the wall is the separation point. Intuitively, the pressure rise (adverse pressure gradient) between the most narrow part and the widest part of the funnel would be highest with a larger divergence angle. Therefore, it is expected that for larger divergence angles the flow would detach after a smaller distance travelled.

In order to measure the separation point, CFD simulations were run for the non-Newtonian fluid for angles ranging from 1 to 45 degrees. The method used to ascertain flow separation is as described in section 3.4.2. The y-coordinate of the slice at which flow separation first developed was obtained as data. The obtained results are shown in figure 4.1.

As can be seen from the plot, as the divergence angle increases, the point of detachment of the flow decreases. This is due to the higher adverse pressure gradient, causing the flow to be able to travel a shorter distance before separating from the wall. Notice that for small angles (1 and 2 degrees) there is no data for the point of flow separation. COMSOL Multiphysics® was unable to find a laminar solution which displayed boundary layer separation for these small angles. Probably the reason for this is a lack of mesh resolution quality. Because the resolution is relatively low, the mesh cells are relatively large. Therefore the cells might be too big to 'see' small vortices at lower volumetric flow rates. The volumetric flow rate is then increased until eventually the flow turns turbulent before flow separation can be noticed. However, it could be possible that for these small angles there is no laminar solution containing flow separation.

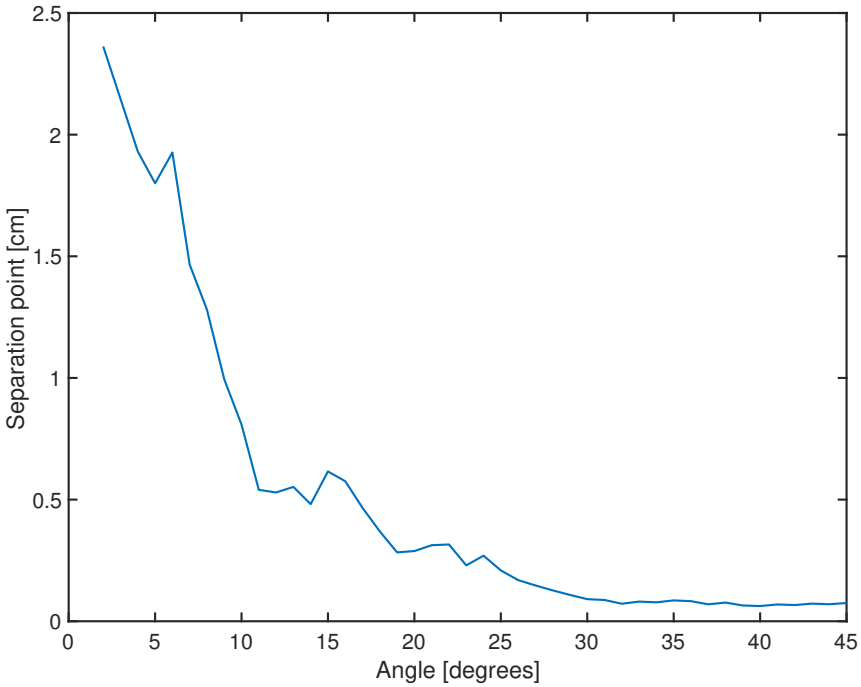

Figure 4.1: Plot of the separation point of boundary layer separation for different divergence angles of the funnel. The separation point is measured from the beginning of the funnel in the y-direction as depicted in figure 3.2

4.2.2 Critical Reynolds number for different angles

The Reynolds number is a well known constant which shows an important indication of the ratio between inertia and friction in the flow. One of the research goals was to study the critical Reynolds number from where flow separation occurs for our electrolyte flow through a diverging funnel and compare this with a Newtonian fluid. The point of interest is if the critical Reynolds numbers for a non-Newtonian fluid and a Newtonian fluid differ significantly and if so, for what reason.

The non-Newtonian electrolyte modeled has the properties as described in section 3.2, and the modeled Newtonian fluid has a constant viscosity of $\mu = 0.3$ $[Pa\ s]$ and density of $\rho = 1000$ $[\frac{kg}{m^3}]$. The density was chosen to be the same as the electrolyte, and the viscosity was chosen the same as oil, since the electrolyte resembles to an oily substance in still form. Simulations were run for different divergence angles for both fluids to obtain solutions for local variables from which the critical Reynolds number could be calculated. The results are depicted in figure 4.2.

As can be seen from the figure, the critical Reynolds number decreases dramatically for both the electrolyte and Newtonian fluid as the divergence angle increases. This can be explained through the adverse pressure gradient, which increases as the divergence

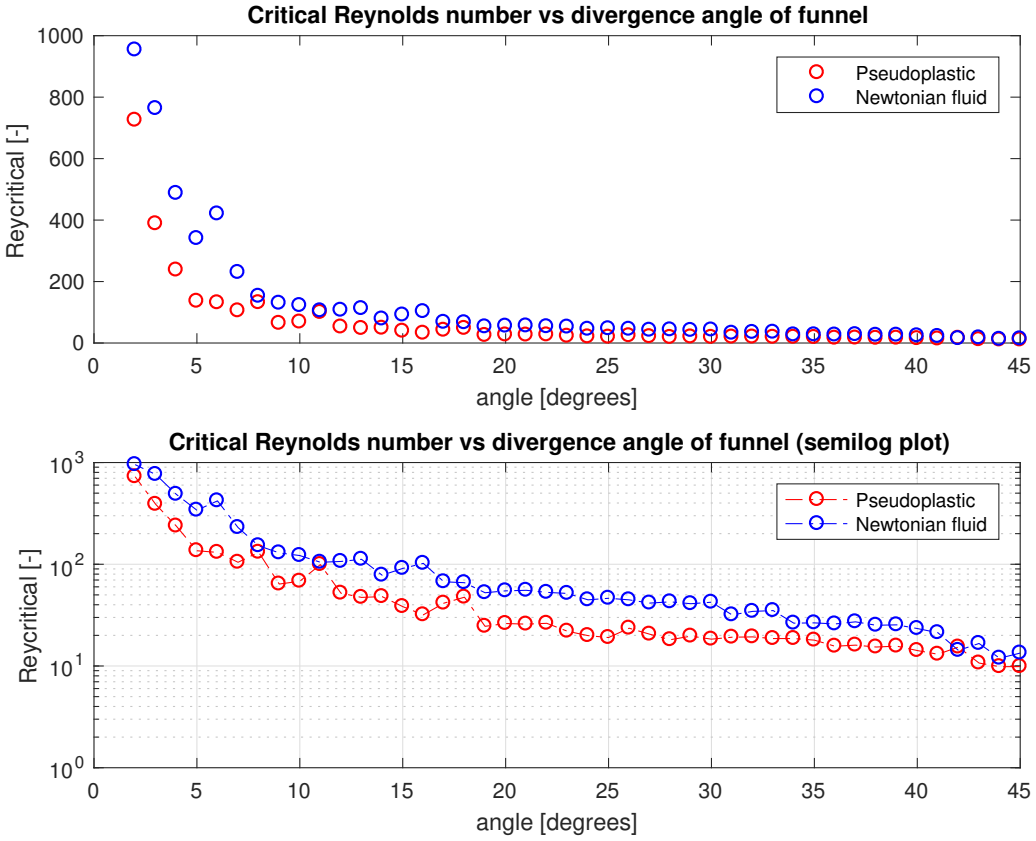

Figure 4.2: Plots of the critical Reynolds number for the electrolyte and a Newtonian fluid. The top plot is a regular plot whereas the bottom plot is plotted on a logarithmic scale on the y-axis.

angle increases. As the funnel diverges, the velocity profile is not only wider but also has less amplitude. The pressure at the edges off the wall at the beginning of the funnel is lower compared to the pressure at the edges of the entrance of the flow cell. This means an adverse pressure gradient, which causes a negative velocity or vortices at the walls.

Figure 4.3 shows that although the absolute pressure difference is smaller for the greater divergence angle compared to the smaller divergence angle, the length over which the pressure increases is far smaller (figures at the same scale). This causes a larger pressure gradient for the funnel with the larger divergence angle. For greater divergence angles, the adverse pressure gradient is high, which causes vortices to develop faster, explaining a lower critical Reynolds number as the divergence angle increases.

From the results of the study it can be concluded that the critical Reynolds number for the electrolyte is lower than for the Newtonian fluid. Again, this is due to the adverse pressure gradient. The velocity profile of pseudoplastics as depicted in figure

2.6 is steeper at the edges of the wall compared to the velocity profile of Newtonian fluids, which means the velocity gradient is high at the edges of the funnel. Referring back to equation 2.4, this would mean a higher adverse pressure gradient compared to Newtonian fluids. Therefore, for lower volumetric flow rates (and thus lower Reynolds numbers) flow separation develops for pseudoplatics compared to Newtonian fluids. It is expected that for dilatant fluids the critical Reynolds number would be even higher than for Newtonian fluids.

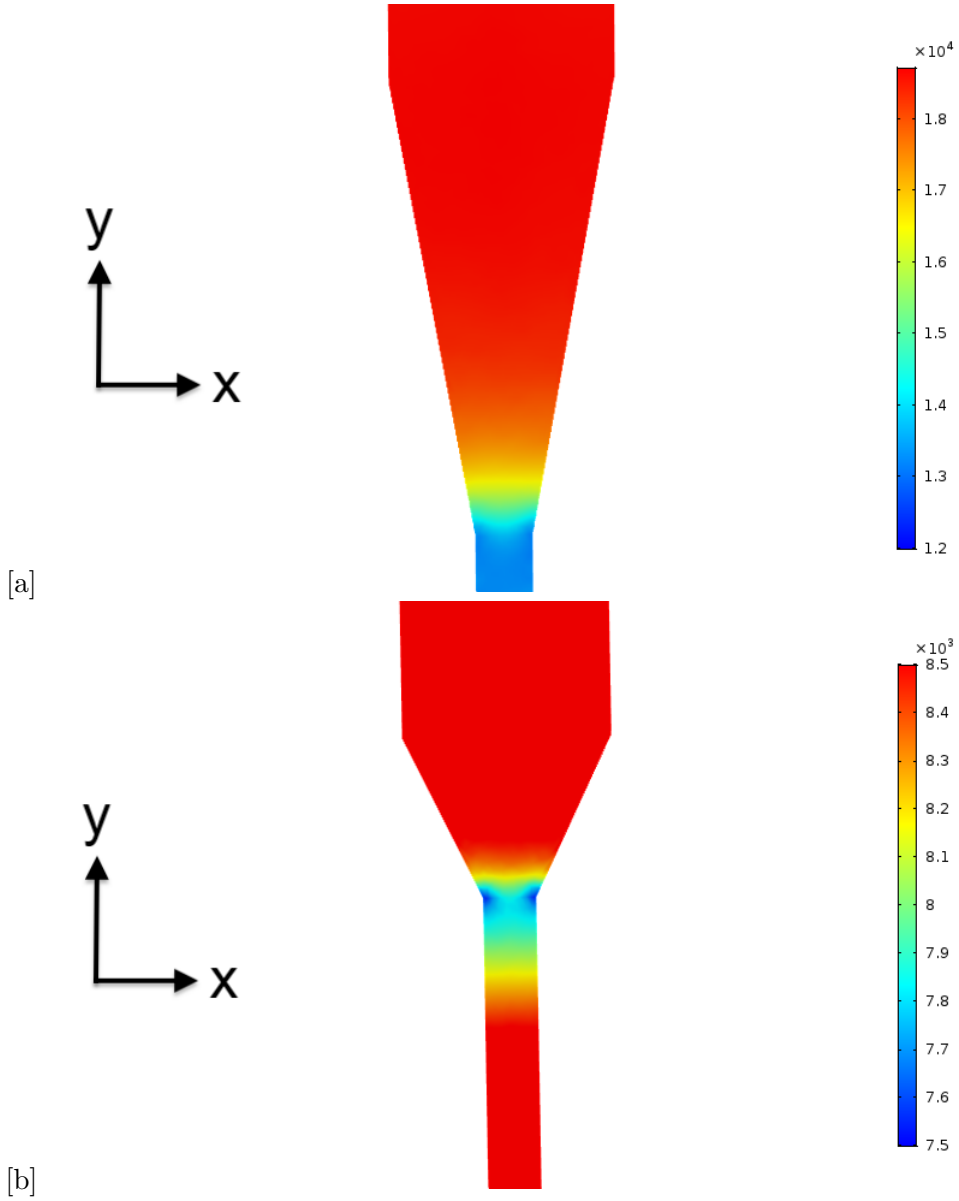

Figure 4.3: Examples of pressure distribution in the funnel (top view), [a] is a funnel with divergence angle θ_d=10 while [b] is a funnel with divergence angle θ_d=25

4.2.3 Critical volumetric flow rate for different angles

The critical Reynolds number is a good indication for when flow separation occurs, not only for this particular geometry but rather in general. However, in order to determine an ideal divergence angle for the flow cell, the interest lies more in the critical volumetric flow rate, since that determines how fast the flow will pass through the cell, and what pumping power is needed to establish such a flow speed. The following figure 4.4 depicts the found critical volumetric rates for the electrolyte and a Newtonian fluid for this particular geometry.

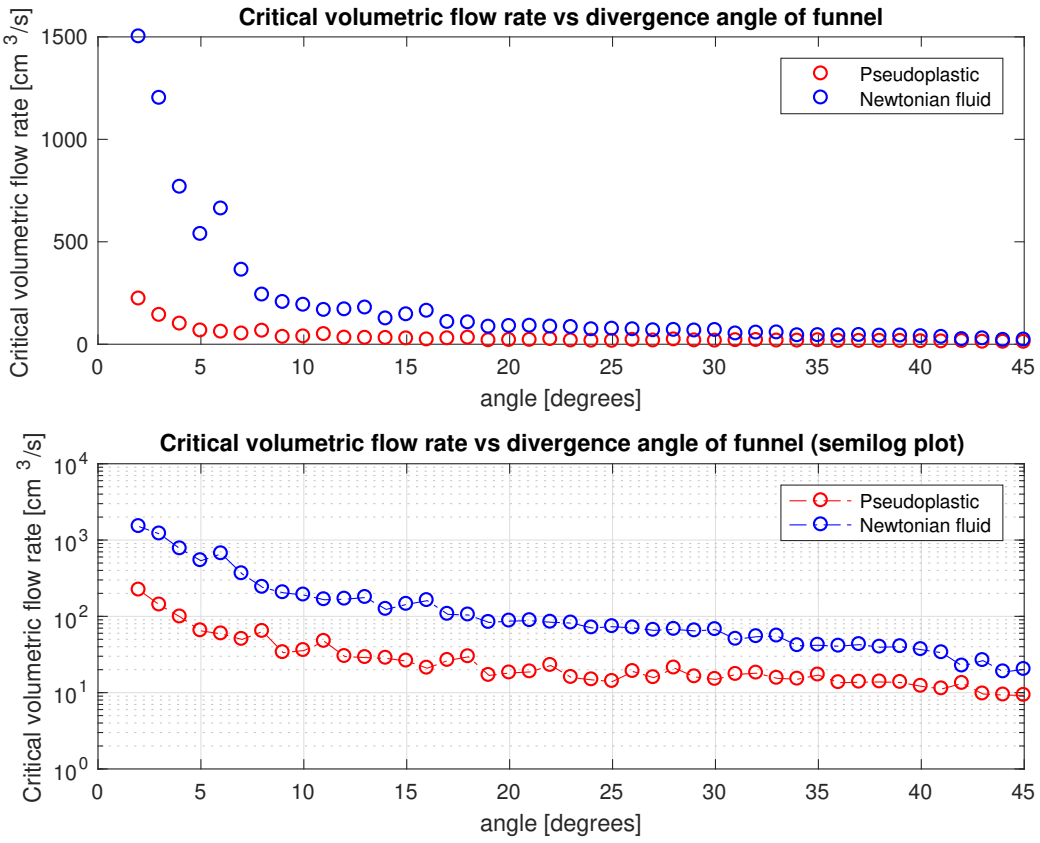

Figure 4.4: Plots of the critical volumetric flow rate for the electrolyte and a Newtonian fluid. The top plot is a regular plot whereas the bottom plot is plotted on a logarithmic scale on the y-axis.

The figure shows a similar distribution to that of the critical Reynolds number. However, the differences between the critical volumetric flow rates for the pseudoplatic and the Newtonian fluid are larger compared to the difference in critical Reynolds numbers. Again, the fact that the critical volumetric flow rate is higher for the Newtonian fluid than for the electrolyte can be explained through a greater adverse pressure gradient.

The larger differences can be explained through the differences in viscosity for the electrolyte over the slice where flow separation first develops. For small angles in particular, the average flow speeds are relatively high, meaning that the apparent viscosity for the electrolyte is relatively low, since it is a shear thinning fluid (see appendix for average viscosities and velocities). Therefore, when integrating over the slice, the average viscosity of the electrolyte is significantly lower than the viscosity of the Newtonian fluid. When looking at the definition of the Reynolds number as in equation 2.7, the volumetric flow rate of the Newtonian fluid must be significantly higher in order to obtain a high Reynolds number. Therefore the differences in critical volumetric flow rates are greater than the differences in critical Reynolds numbers, especially for small angles.

4.3 Cell shape impact

In order to not only study the influence of the divergence angle on flow separation, an additional set of simulations was conducted to study the influence of the flow cell geometry. The method used is as described in section 3.4.3. The results are depicted in figure 4.5.

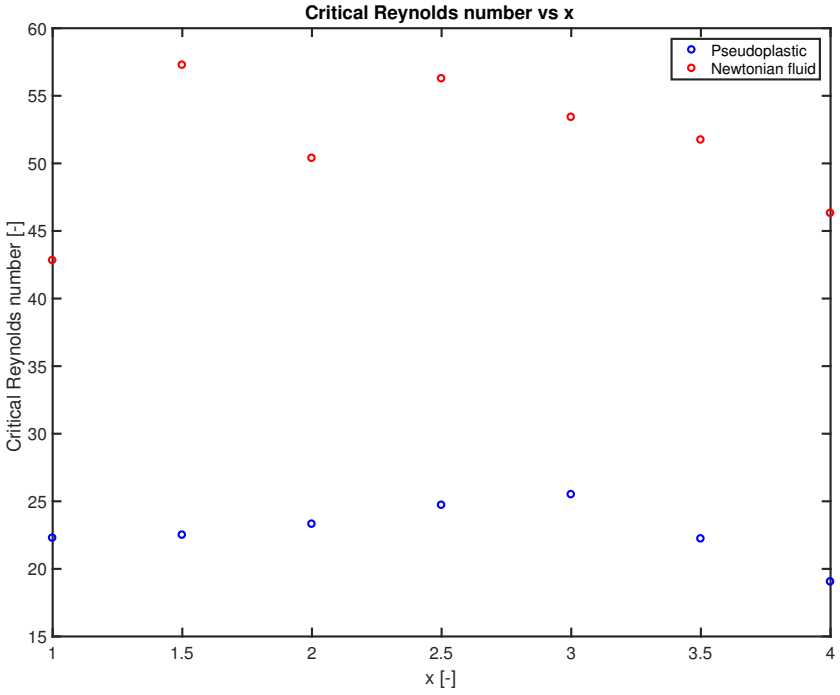

Figure 4.5: Plot of the critical Reynolds number for a divergence angle of 25 degrees and different ratios x $[-]$ between width and height of the flow cell while maintaining a constant hydraulic diameter D_h=0.8 for the flow cell.

The results show a pattern which is not very coherent with what would be expected from theoretical point of views. It is expected that for a square flow cell, the critical Reynolds number would be high, most symmetric surface. Therefore, a square would mean that the maximum velocity gradient at the edges would be low compared to more stretched out surfaces. This would mean the that the adverse pressure gradient of the square would be lower than for more rectangular surfaces. However, the results do not seem to show such a pattern. Furthermore, the pattern of the results for the electrolyte and a Newtonian fluid do not match perfectly. Possibly the pattern could be explained by the shear-thinning nature of the electrolyte, which could mean odd velocity and pressure gradients at the corners of the square or rectangle. However, the mesh resolution could also play a role in the incoherent patterns.

Chapter 5

Design of the flow cell

In this chapter, the eventual design of the experimental setup of the flow cell will be discussed. It is important to note that due to time pressure, a design had to be presented before the whole of the research could be conducted. The first section will discuss the design of the flow cell including the funnels. The second section will discuss other components of the experimental setup.

5.1 Dimensions flow cell

As mentioned in subsection 3.1.1, the dimensions of the flow cell are 10 cm by 2 cm by 0.5 cm. These dimensions were chosen in consultation with dr. Hlongwa, considering mainly the maximum amount of electrolyte volume and design used in other conducted studies. The total volume of the cell is 10 cm^3, and it has a surface of 1 cm^2.

5.2 Divergence angle funnel

Unfortunately, the design for the flow cell including the funnels had to be made before the whole study could be finalized. Therefore, only a part of the simulations could be conducted. The choice for the divergence angle was based on these simulations, in combination with information from literature. In order to study the effects of the flow on the electrochemical reaction, several flow rates should be possible. Based on the literature, the choice was made for a divergence angle of θ_d= 25 degrees [6] [16] [17] [19]. With this divergence angle, the critical volumetric flow rate would be 14 $\frac{mL}{s}$ which can be seen in figure 4.4. This divergence angle would allow the flow cell to be flowed through in a less that one second, which, according to previous research would mean a relatively high flow speed. Furthermore, a divergence angle of 25 degrees would have a volume of approximately 1 cm^3, which is quite small. The optimal divergence however would be θ_d= 41 degrees, which would allow the flow cell to be flowed through in 1 second at maximum volumetric flow rate. While this is relatively still a very high flow velocity compared to previous studies [18] [19], it is an easy to work with upper limit

for test purposes. Furthermore, the funnel would have a volume of 0.53 cm^3, meaning less volume of electrolyte is needed for the entire system.

5.3 Separator

In between the two half cells a separator is placed allowing the ions to diffuse between the electrolytes without leakage. The used separator is a filter paper made by the company Whatman®. The filter paper is the 'Whatman® quantitative filter paper, hardened ashless, Grade 542'. The filter paper has a pore size of 2.7μm and is 150μm thick [22].

5.4 3D print

After completing the design, it was sent to Dienst Elektronische en Mechanische Ontwikkeling (DEMO) to 3D print the flow cell block. The first prototype has been printed. A slight adjustment has been made in order to realize a perfect flow cell. As turned out, there was not enough vertical space between inlet and outlet to connect both to the tubing. Therefore, the inlets and outlet were shifted, by creating funnels which diverge only on one side. This way, the same divergence angle is used and it is possible to connect the inlets and outlets to the tubing. The new design is depicted in figure 5.1. The eventual 3D printed prototype can be observed in figure 5.2 on the next page.

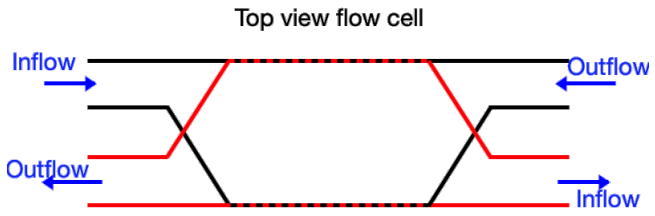

.

Figure 5.1: Schematic depiction of the top view of the adjusted flow cell design. Red indicates one half cell whereas black indicates the other half cell

Figure 5.2: Picture of the 3D printed prototype of half of the flow cell block.

Chapter 6

Conclusion and recommendations

The main research goal was to study the flow of a Non-Newtonian fluid through a diverging funnel, for the purpose of designing an experimental setup to study the effect of flow on the electrochemical reaction of an SSFB. The research focused on the development of boundary layer separation in the funnel.
By modeling the flow cell with the standard dimensions and varying the divergence angle of the funnel the separation point could be studied. As expected, the length the flow had to travel before the boundary layer separated decreased as the divergence angle increased. This can be explained by the adverse pressure gradient, which increases as the divergence angle increased. For higher adverse pressure gradients the fluid flow separated from the boundary layer after travelling a shorter distance.
For the purpose of designing an experimental setup to study the effect of flow on the electrochemical reaction of an SSFB, the critical Reynolds number was of importance. The flow cell with standard dimensions were modeled for different divergence angles. The results showed that as the divergence angle increased, the critical Reynolds number dramatically decreased, which is in accordance with literature [16]. The electrolyte experienced lower critical Reynolds numbers than a standard Newtonian fluid, which can be explained by the less sharp velocity profile of the electrolyte. This causes higher adverse pressure gradients at the walls leading to flow separation developing quicker.
Unfortunately, the results for modeling the funnel and flow cell for different flow cell shapes with constant hydraulic diameter did not yield consistent outcomes. This possibly could be explained by odd velocity and pressure gradient at the walls, or possibly by a lack in mesh resolution.
For further research, it is recommended that a finer mesh is applied to the model. The quality and accuracy of the results could be improved when applying a mesh with higher resolution. Moreover, a study combining the influence of the cell geometry and the divergence angle would sketch a wider image of non-Newtonian fluid flow through diverging channels. Furthermore, it would be interesting to study the flow of dilatant fluids through diverging funnels, which is beyond the scope of this research.

Bibliography

[1] Richard Gray. The biggest energy challenges facing humanity. http://www.bbc.com/future/story/20170313-the-biggest-energy-challenges-facing-humanity, 2017.

[2] Adam Z Weber, Matthew M Mench, Jeremy P Meyers, Philip N Ross, Jeffrey T Gostick, and Qingua Liu. Redox flow batteries: a revies. *Journal of applied electrochemistry*, 2011.

[3] Liang Su, A Kowalski, Kyler J Carroll, and Fikile R Brushett. Recent developments and trends in redox flow batteries. *Green energy and technology*, 2015.

[4] Mihai Duduta, Bryan Ho, Vanessa C Wood, Pimpa Limthongkul, Victor E Brunini, W Craig Carter, and Yet-Ming Chiang. Semi-solid lithium rechargable flow battery. *Advanced energy materials*, 1(4):511–516, 2011.

[5] Colin Qi and Gary Koenig. Review article: Flow battery systems with solid electroactive materials. *Journal of Vacuum Science and Technology B: Nanotechnology and Microelectronics*, 35:040801, 07 2017.

[6] Victor E. Brunini, Yet-Ming Chiang, and W. Craig Carter. Modeling the hydrodynamic and electrochemical efficiency of semi-solid flow batteries. *Electrochimica Acta*, 69:301 – 307, 2012.

[7] Balancing redox reaction by ion electron method (basic medium). https://chemistryonline.guru/redox-reaction/. Accessed: 2019-01-07.

[8] Ntuthuko Hlongwa. Personal interview, 07 2019.

[9] Mohamed Youssry, Fadi Z. Kamand, Musaab I. Magzoub, and Mustafa S. Nasser. Aqueous dispersions of carbon black and its hybrid with carbon nanofibers. *RSC Adv.*, 8:32119–32131, 2018.

[10] Johannes Lohaus, Deniz Rall, Maximilian Kruse, Viktoria Steinberger, and Matthias Wessling. On charge percolation in slurry electrodes used in vanadium redox flow batteries. *Electrochemistry Communications*, 101:104 – 108, 2019.

[11] Mohammad Arjmand. *Electrical Conductivity, Electromagnetic Interference Shielding and Dielectric Properties of Multi-walled Carbon Nanotube/Polymer Composites*. PhD thesis, 02 2014.

[12] Harry Van den Akker and R.F. Mudde. *Transport Phenomena - The Art of Balancing*. 08 2014.

[13] Non-newtonian models. https://www.simscale.com/docs/simulation-setup/model/materials/non-newtonian-models/. Accessed: 2019-06-28.

[14] Melissa M. Simpson and William Janna. Newtonian and non-newtonian fluids: Velocity profiles, viscosity data, and laminar flow friction factor equations for flow in a circular duct. *ASME International Mechanical Engineering Congress and Exposition, Proceedings*, 9, 01 2008.

[15] P. M. Eagles. The stability of a family of jeffery–hamel solutions for divergent channel flow. *Journal of Fluid Mechanics*, 24(1):191–207, 1966.

[16] Mamta Jotkar, Gayathri Swaminathan, Kirti Sahu, and Rama Govindarajan. Global linear instability of flow through a converging-diverging channel. *Journal of Fluids Engineering*, 138, 08 2015.

[17] Kirti Sahu and Rama Govindarajan. Stability of flow through a slowly diverging pipe. *Journal of Fluid Mechanics*, 531, 09 2004.

[18] Minjoon Park, Jaechan Ryu, Wei Wang, and Jaephil Cho. Material design and engineering of next-generation flow-battery technologies. *Nature Reviews Materials*, 2:16080, 12 2016.

[19] Edgar Ventosa, Osemudiamen Amedu, and Wolfgang Schuhmann. Aqueous mixed-cation semi-solid hybrid-flow batteries. *ACS Applied Energy Materials*, 1(10):5158–5162, 2018.

[20] Kudakwashe Chayambuka, Jan Fransaer, and Xochitl Dominguez-Benetton. Modeling and design of semi-solid flow batteries. *Journal of Power Sources*, 434:226740, 2019.

[21] What is a mesh? https://www.simscale.com/docs/content/simwiki/preprocessing/whatisamesh.html. Accessed: 2019-04-07.

[22] Whatman® quantitative filter paper, hardened ashless, grade 542. https://www.sigmaaldrich.com/catalog/product/aldrich/wha1542185?lang=enregion=NL. Accessed: 2019-07-16.

Chapter 7

Appendix

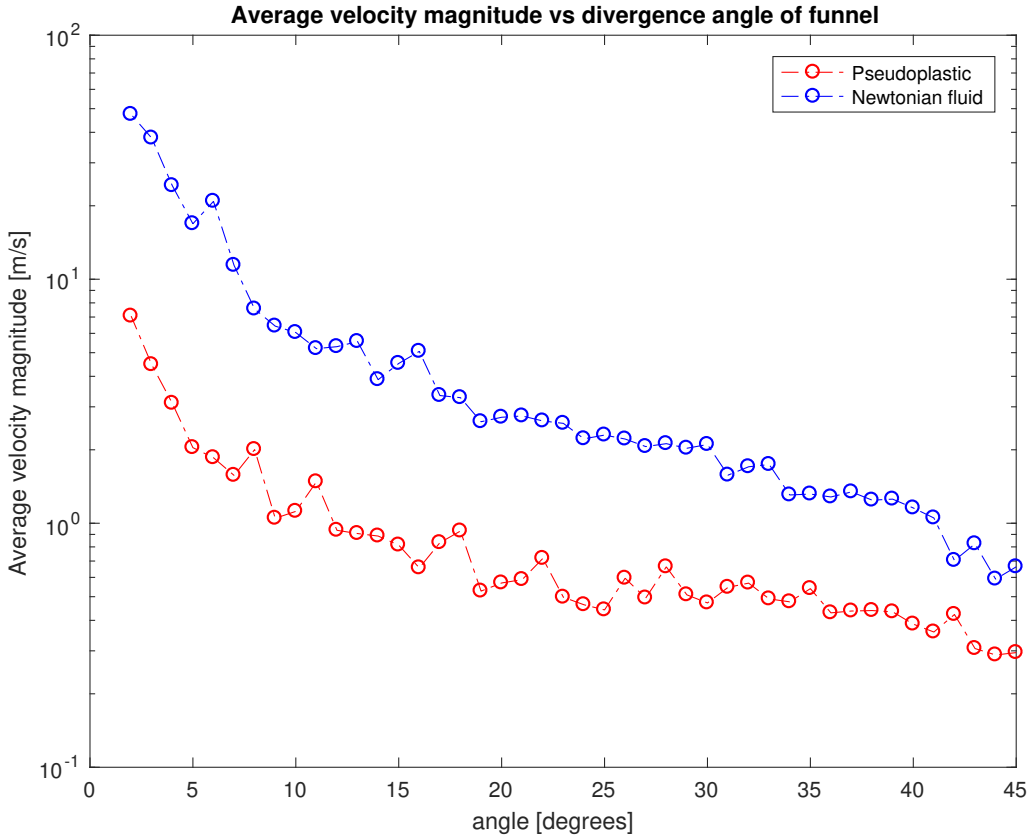

Figure 7.1: Average velocity magnitude at the critical Reynolds number for different angles.

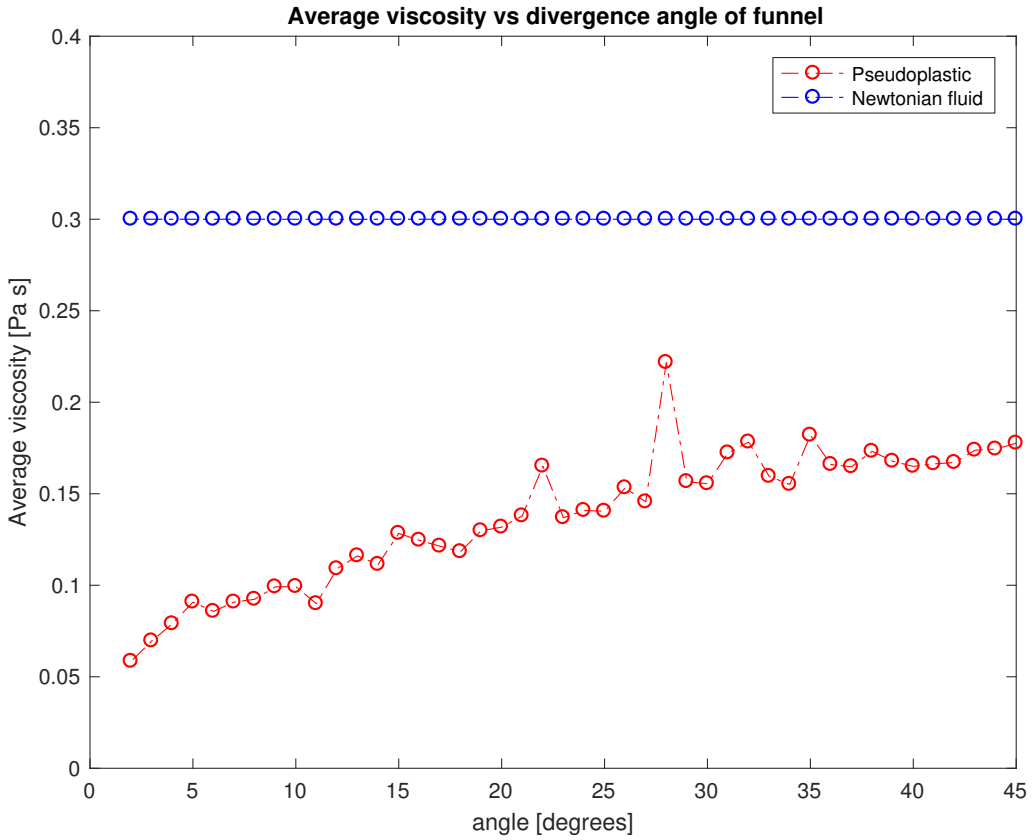

Figure 7.2: Average viscosity at the critical Reynolds number for different angles.